Fuel Processing Technology 128 (2014) 310–318

Contents lists available at ScienceDirect

Fuel Processing Technology

journal homepage: www.elsevier.com/locate/fuproc

Effect of environment around the active center Cu^+ species on the catalytic activity of CuY zeolites in dimethyl carbonate synthesis: A theoretical study

Huayan Zheng [a], Jun Qi [a], Riguang Zhang [a], Zhong Li [a,*], Baojun Wang [a,*], Xinbin Ma [b]

[a] Key Laboratory of Coal Science and Technology of Ministry of Education and Shanxi Province, Taiyuan University of Technology, Taiyuan 030024, Shanxi, China
[b] Key Laboratory for Green Chemical Technology of Ministry of Education, Tianjin University, Tianjin 300072, China

ARTICLE INFO

Article history:
Received 31 March 2014
Received in revised form 24 July 2014
Accepted 24 July 2014
Available online xxxx

Keywords:
Dimethyl carbonate
CuY zeolite
Environment
Cs
Density functional theory

ABSTRACT

A density functional theory method has been used to investigate the effect of environment around the active center Cu^+ species on the catalytic activity in the oxidative carbonylation of methanol to dimethyl carbonate over CuY zeolites. Based on the configuration of Cu^+ located in the supercage, Cu^+ or Cs^+ species at the sites adjacent to the active center Cu^+ species in the supercage are considered as the surrounding environment. The results indicate that the presence of Cu^+ in the supercage adjacent to the active center improves the adsorption energy of co-adsorbed CO and elongates the $Cu-OCH_3$ bond in co-adsorbed CO/CH_3O system, stabilizes the transition state for the reaction of CO insertion, and ultimately makes the active center Cu^+ species exhibit better catalytic activity. Whereas, Cu^+ species at adjacent site in the smallcage plays an opposite role. More importantly, introducing Cs species into the supercage of CuY zeolite significantly improves the adsorption energy of co-adsorbed CO and the stability of transition state configuration for CO insertion reaction, thus, leads to the best catalytic performance among four types of catalysts, which is consistent with the previous experimental results.

1. Introduction

Dimethyl carbonate (DMC) is a good oxygenated fuel additive of gasoline or diesel oil to replace methyl tert-butyl ether (MTBE) [1–5]. Adding DMC to fuels can significantly increase the octane number due to its high oxygen content (53.3 wt.%), and also obviously improve the vaporization of diesel fuel by reducing their surface tension. Another obvious advantage of DMC as fuel additives is that it slowly decomposes to form CO and methanol, which have no serious impact when released into the environment [1]. This and other applications led to an enormous effort in the investigation of low-cost and nontoxic synthesis of DMC.

Among all the reactions to DMC, the oxidation carbonylation of methanol to DMC has received great attention due mostly to its beneficial thermodynamics and atom utilization rate of 80% [6–8]. At present, the main catalysts for the DMC synthesis include the supported copper chloride ($CuCl_2$) catalyst, Wacker catalyst and Cu-exchanged zeolite catalyst [1]. However, for the supported $CuCl_2$ catalyst and Wacker catalyst, the loss of chloride results in catalyst inactivation and equipment corrosion [8,9]. Consequently, Cu-exchanged zeolite catalysts, as the chloride-free catalysts, have been considered as one of the most potential catalysts for application in the DMC synthesis in recent years [7,10–14]. Nowadays, Cu-exchanged zeolite catalysts, such as CuY [10,13,15–18], CuX [11,12], Cu-ZSM-5 [7,11,13], Cu-MOR [13] and Cuβ [14], have been widely used to catalyze the oxidation carbonylation of methanol to DMC. Among these catalysts, CuY zeolite exhibits the highest catalytic activity and selectivity for the oxidative carbonylation of methanol to DMC [13].

CuY zeolite was generally prepared by the ion-exchanged method or incipient–wetness–impregnation, then activated at 600–750 °C in inert atmosphere [18–20], and found that high temperature treatment is necessary to allow for auto-reduction of Cu^{2+} to Cu^+ and the migration of copper species from supercages to sodalite cages or hexagonal prisms of the faujasite structure [18–22]. As reactant molecule, CO is very difficult to diffuse inside the sodalite cages and hexagonal prisms (2.3 Å) [23] of Y zeolite because of its large dynamic diameter (3.76 Å) [24], while they are easy to enter supercages (7.4 Å) [23], suggesting that only Cu^+ species in the supercage act as the active sites for the oxidative carbonylation of methanol to DMC [6,18,25].

Previous literatures [6,10,15,17,26] have reported the reaction mechanism for the oxidative carbonylation of methanol to DMC over Cu^+ species in the supercage of Y zeolite. For example, Zheng and Bell [6] have selected the 6T atom cluster for one Cu^+ cation associated with site II in the supercage to investigate the mechanism of DMC synthesis, and found that the molecularly adsorbed methanol is oxidized by oxygen to either mono-methoxide or di-methoxide species; then the

* Corresponding authors at: No. 79 Yingze West Street, Taiyuan 030024, China. Tel./fax: +86 351 6018526.
E-mail addresses: lizhong@tyut.edu.cn (Z. Li), wangbaojun@tyut.edu.cn (B. Wang).

http://dx.doi.org/10.1016/j.fuproc.2014.07.037
0378-3820/

formation of DMC derives from two distinct reaction pathways: one is the insertion of CO into mono-methoxide to CH_3OCO species, subsequently CH_3OCO rapidly reacts with CH_3OH to DMC; and another involves that DMC is formed by the CO addition to di-methoxide species. All the studies [6,10,15,17,26] suggested that CO insertion into CH_3O to CH_3OCO is the rate-limiting step of oxidative carbonylation of methanol to DMC.

In fact, there are numerous Cu species located at the sites in CuY zeolite, mainly including sites I′ (I), II (II*), and III (see Fig. 1) [21,25,27,28]. The presence of Cu^+ or other metal cations at the sites adjacent to the active center Cu^+ generally results in different environments. Our group experimentally found that the introduction of Cs species changed the environment around the active center Cu^+ species, and improved the space time yield of DMC over CuY zeolite [29]. Kieger et al. [30] and Ribeiro et al. [31] have obtained a similar effect of introducing Cs species into CuY zeolite. However, up to now, little is known about the effect of the environment around the active site on the catalytic activity of CuY zeolites.

In this study, we employ density functional theory (DFT) calculations to investigate how the presence of Cu^+ or Cs^+ cation, at the site adjacent to the active center, influences the environment around the active center Cu^+ species of CuY zeolite and its catalytic activity in DMC synthesis. The insertion of CO to methoxide species was chosen to evaluate the catalytic activity, since it is the rate-limiting step of oxidative carbonylation of methanol to DMC [6,10,15,17,26]. Firstly, an appropriate size of clusters was adopted to construct the stable configurations of CuY zeolites with different environments. Secondly, based on the stable configurations, the associated performances of the active center Cu^+ species have been considered and discussed in detail. Finally, our obtained results should provide the fundamental mechanisms of enhanced catalytic activity for CuY zeolites applied in the DMC synthesis field.

2. Computational details

2.1. Computational methods

Density functional theory calculations were performed using the DMol^3 program package of Materials Studio 4.4 [32]. The generalized-gradient approximation (GGA) with the Perdew–Burke–Ernzerhof (PBE) exchange-correction functional was used to perform for all calculations [33]. The double numerical plus polarization (DNP) basis set [34], which is equivalent in accuracy to the commonly used 6-31G** Gaussian basis set, was used throughout the calculations. In this calculation, Si, O, H and C atoms were treated with all electron basis sets, while the inner electrons of the Al, Cu and Cs atoms were kept frozen and replaced by an effective core potential (ECP). The convergence criteria were set to be 2×10^{-5} Ha for energy, 4×10^{-3} Ha/Å for force, and 0.005 Å for displacement. Complete linear synchronous transit (LST) and quadratic synchronous transit (QST) were used to determine the transition state (*TS*).

For the reaction $CO + CH_3O \rightarrow CH_3OCO$ on CuY zeolite, the reaction energy (ΔH) and activation barrier (E^a) are calculated as follows:

$$\Delta H = E_{CH3OCO/CuY} - E_{CO+CH3O/CuY}$$
$$E^a = E_{TS/CuY} - E_{CO+CH3O/CuY}$$

where $E_{CH3OCO/CuY}$ is the total energy for the product CH_3OCO on CuY zeolite; and $E_{CO\ +\ CH3O/CuY}$ and $E_{TS/CuY}$ represent the total energies of the co-adsorbed CO and CH_3O on CuY zeolite and the transition state (*TS*) on CuY zeolite, respectively. The negative value of ΔH represents that the reaction is exothermic.

In addition, the binding energy of Cu^+ species (E_{bind}) in Y zeolite is calculated as follows [35]:

$$E_{bind} = E_{Cu} + E_Y^- - E_{CuY}.$$

Here, E_{Cu} represents the energy of single Cu^+; and E_Y^- and E_{CuY} are the total energies of Y^- and CuY systems, respectively. The larger the value of E_{bind} is, the more stable the structure of Cu-exchanged zeolite system is.

The adsorption energy (E_{ads}) of the adsorbate–cluster system is defined as follows:

$$E_{ads} = E_{adsorbate} + E_{CuY} - E_{adsorbate/CuY}$$

where $E_{adsorbate}$ is the energy of adsorbate; and E_{CuY} and $E_{adsorbate/CuY}$ represent the total energies of the CuY cluster and adsorbate–CuY zeolite systems in the stable state. With this definition, the large adsorption energy indicates the strong interaction between the adsorbate and CuY zeolite.

2.2. Cluster model

The cluster approach, which allows for the use of high quality theoretical methods to describe the local conformations and interactions of molecules [6,16,25,36], was adopted. The geometry of the zeolite cluster model used in this work was taken from the framework structure of FAU. The dangling bonds near Al atoms were terminated by SiH_3 groups, and others were saturated by H atoms [25,37]. The terminal atoms were oriented along the bond direction as Y zeolite, and the bond length of Si–H and O–H bonds was set to 1.5 and 1.0 Å, respectively. In order to keep the local structure of Y zeolite during the optimization, for Y^-, CuY, MY^- and CuMY (M is used to represent Cu or Cs) cluster models, the compensating charges, the Al atoms and the adjacent SiO_4 atoms were relaxed, while other atoms were fixed; for adsorbate–CuY cluster system, the compensating charges, the absorbed molecules and the 6MR occupied by the active center Cu^+ species were relaxed.

In general, the calculation is sensitive to the size of cluster, and a cluster being too small may result in artifacts [38]. Consequently, it is necessary to find the right size of cluster for our study. For active site II in the supercage, the different sized clusters, consisting of 8T, 13T, 24T, 31T, 36T, 42T and 60T atoms (T is used to represent Al or Si atom) (see Fig. 2), were used. The binding energies of Cu^+ species in different sized Y clusters and the adsorption energies of CO on CuY zeolite

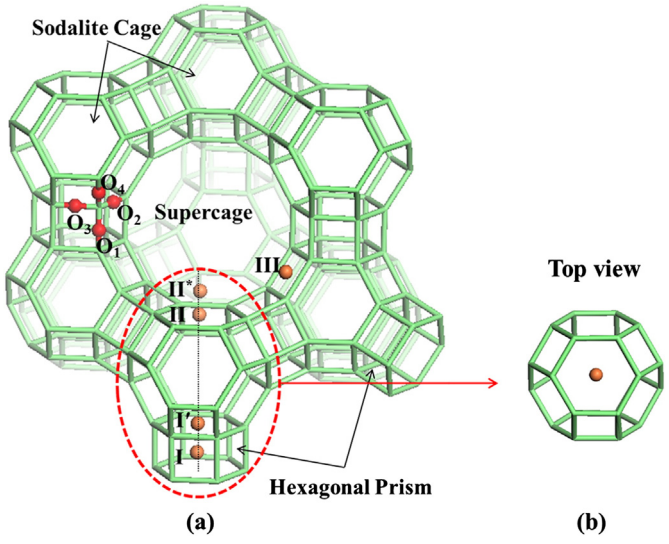

Fig. 1. The structure of faujasite. (a) Faujasite type structure with cationic sites (orange balls) and different crystallographic oxygen positions (red balls); (b) the top view of faujasite in the oval-shaped rings. Site I′ is in the sodalite cage adjacent to six membered ring (6MR) shared by a sodalite cage and a hexagonal prism; site I is at the center of the hexagonal prism; site II is in the supercage adjacent to a 6MR shared by a sodalite cage and a supercage; site II* is like site II, but toward the supercage; site III is in the supercage adjacent to four membered ring (4MR) of a sodalite cage. (For interpretation of the references to color in this figure legend, the reader is referred to the web version of this article.)

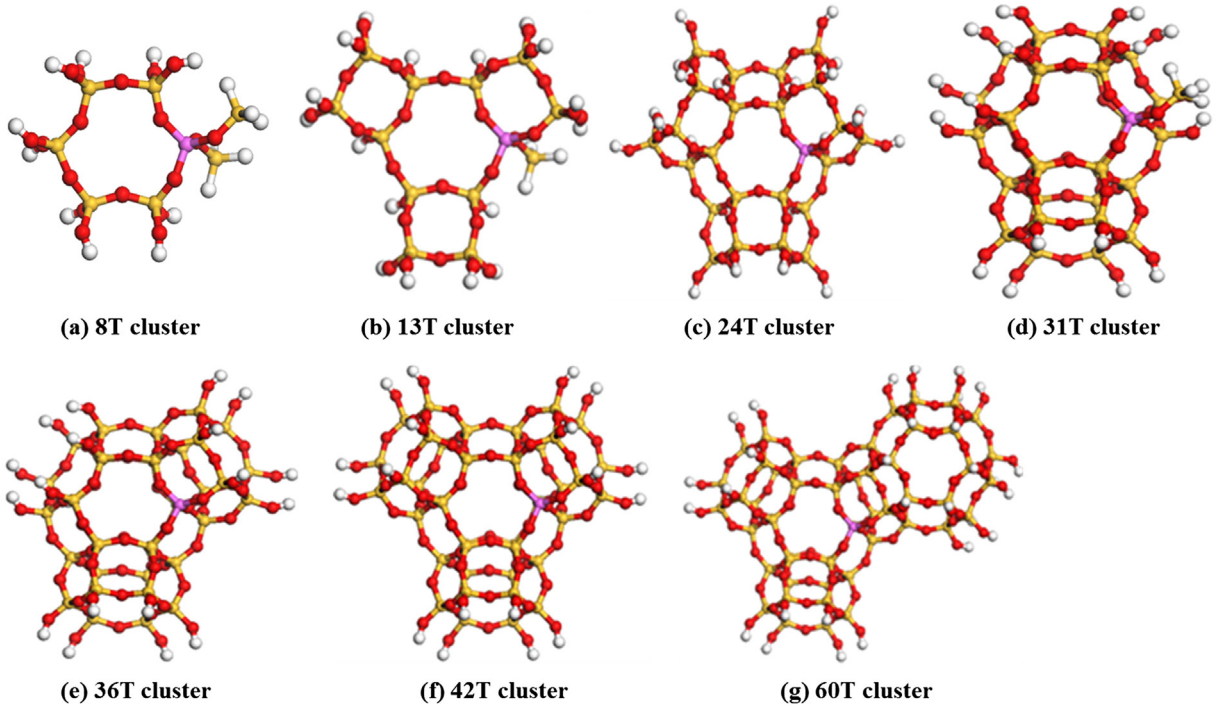

Fig. 2. The cluster geometries of Y zeolite with different sizes. Red, yellow, pink and white balls stand for O, Si, Al and H atoms, respectively. (For interpretation of the references to color in this figure legend, the reader is referred to the web version of this article.)

with different sized clusters are studied, as shown in Fig. 3. It can be found that the effect of the size on the adsorption energies of CO is negligible, while the Cu^+ binding energies are significantly influenced by the size, suggesting that too small cluster model cannot fully reflect the structure of Y zeolite. Meanwhile, in order to investigate the effect of Cu^+ species in the smallcage, the cluster model of Y zeolite should contain a sodalite cage and a hexagonal prism. Comparison of the Cu^+ binding energies of the clusters with different sizes reveals that the difference between 31T cluster and the larger cluster (60T cluster) is negligible (see Fig. 3). Taking the computational cost into consideration, the 31T cluster model including a sodalite cage and a hexagonal prism has been adopted in this study, which is similar with the cluster model of the reference [16,36]. To reflect the Y zeolite with Si/Al = 5.3 used in the experimental study, 5 Si atoms are replaced by Al atoms, which

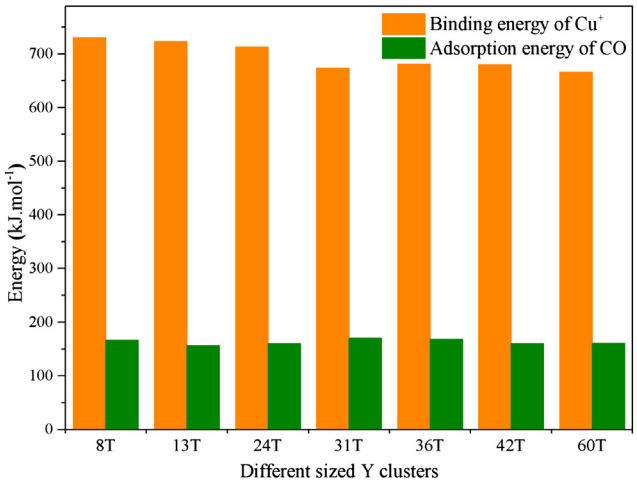

Fig. 3. The binding energies (E_{bind}) of Cu^+ and the adsorption energies (E_{ads}) of CO on the clusters of CuY zeolites with different sizes.

are distributed according to our previous work [16]. The stable structure of cluster model is shown in Fig. 4, and the locations of Al atoms have been marked. Due to the replacement of Si atoms by Al atoms, negative charges are introduced and usually compensated by protons coordinated with crystallographic oxygen atoms adjacent to the Al atoms. There are four crystallographic oxygen positions in Y zeolite (see Fig. 1). O1H with the proton points to the supercage; O2H with the proton is located inside the 6MR shared by a sodalite cage and a supercage; O3H with the proton points to the inside of a 6MR shared by a sodalite cage and a hexagonal prism, and O4H with the proton points to the inside of a twelve-membered ring of a supercage. According to the literatures [35,39–41], a majority of charge-compensating protons are located at O1 sites, while the others occupy O3 sites to avoid the formation of $-OH_2$ group. In this study, for Y zeolite with five Al atoms, three charge-compensating protons are located at O1 sites, and two protons are at O3 sites (see Fig. 4); for CuY zeolite, Al atoms are compensated by four protons and one Cu^+ cation; for CuMY zeolite, only three protons, one Cu^+ cation and one M^+ cation are used to compensate the five Al atoms.

2.3. The stable configurations of CuY zeolite with different environments

The results show that Cu^+ species at site I shift to the plane of 6MR shared by sodalite cage and hexagonal prism after optimization, and the stable structures are similar to the structure of Cu^+ at site I′; similarly, the Cu^+ species located at site II* move to the site II, which is adjacent to a 6MR shared by a sodalite cage and a supercage. The configuration of Cu^+ at site I′ near Al3 atom is listed in Fig. 5(a), and Cu^+ at site I′ near other Al atoms is close to Fig. 5(a); similarly, the configuration of Cu^+ at site II near Al2 atom is shown in Fig. 5(b), and Cu^+ at site II near other Al atoms is alike in Fig. 5(b). While there are two types of configurations for Cu^+ at site III: one is that Cu^+ species, coordinated with one O1 atom and one O4 atom, are located at the edge of two 4MRs (see Fig. 5(c)); another is that Cu^+ species bind to two O4 atoms above a 4MR (see Fig. 5(d)), which is more stable than the former. In addition, the average length of Cu–O and Cu–Al bonds of Cu at several cationic

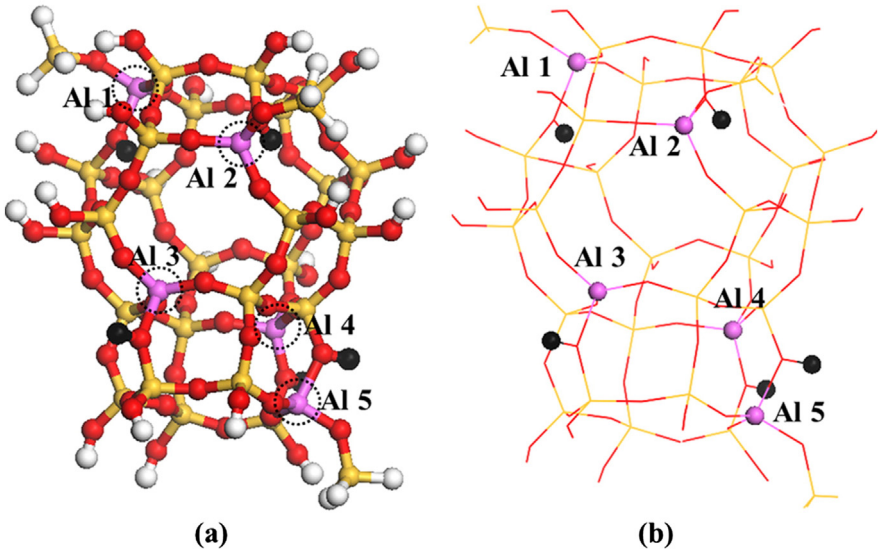

Fig. 4. Cluster geometry with a sodalite cage and a hexagonal prism of Y zeolite. (a) The cluster with ball and stick; (b) the cluster with ball and line. Black balls represent the locations of compensating protons; red, yellow, white and pink balls stand for O, Si, H and Al atoms, respectively. (For interpretation of the references to color in this figure legend, the reader is referred to the web version of this article.)

sites is close to the experimental results of Drake et al. [25], which shows that our calculation is credible.

As seen in Table 1, the binding energies of Cu^+ decrease in the following order of site I′ > site II > site III, indicating that site I′ is the most stable location for Cu^+ species in the Y zeolite, which explains the phenomenon that the exchanged Cu^+ species in the supercage migrate into the smallcage during the high-temperature calcination [18,29]. It can be also found that the majority of Cu^+ species in the surpercage are located at site II, which also prove the experimental results [25] that 17.2 and 33.3 Cu cations are present at site II and site I′ per unit cell, respectively, but only 3.4 Cu/unit cell is located at site III. Therefore, site II and site I′ were selected as the location of Cu^+ species in the supercage and smallcage, respectively. Due to the aperture size of the sodalite window (2.3 Å) [23], Cs^+ cation with an ionic radius of 1.67 Å [42] has a hindered access to the sodalite cage, so Cs^+ cation can only be located in the supercage [31,42,43]. Frising and Leflaive [42] further pointed out that Cs^+ cation only occupied site II* in Y zeolite. In this study, site II* was chosen as the location of Cs^+ cation.

In order to illuminate easily, sites I′, II, and II* adjacent to the active center Cu^+ at site II are denoted as I'_a, II_a, and II_a^* (see Fig. 6), respectively. Cu^+ at II_a or I'_a and Cs^+ at II_a^* will lead to different environments around the active center. Thus, four configurations of $Cu_{II}Y$, $Cu_{II}Cu_{IIa}Y$, $Cu_{II}Cu_{I'a}Y$, and $Cu_{II}Cs_{IIa^*}Y$ are constructed to reflect the different types of environments (see Fig. 7).

3. Results and discussion

3.1. The nature of the active center Cu^+ species

As Table 2 lists, the net charges of Cu^+ decreases from 1.0 *e* of isolate Cu^+ to 0.3–0.4 *e* of CuY zeolites with different environments, which attributes to the electrons transfer from Y zeolite to Cu^+ species [44–46]. Similar results are gained on Cu^+ at different locations of Y zeolite from Table 1. Relative to that (0.358 *e*) of $Cu_{II}Y$ zeolite, the net charge of the active Cu in $Cu_{II}Cu_{I'a}Y$ zeolite increases to 0.393 *e* due to the decreasing populations of 4s and 4p. The similar result is also found on $Cu_{II}Cs_{IIa^*}Y$ zeolite. While for $Cu_{II}Cs_{IIa^*}Y$ zeolite, the net charge (0.345 *e*) of the active Cu is lower than $Cu_{II}Y$ zeolite, which is related to the slight decrease of 3d and 4p populations, and the increasing populations of 4s. It can also be found that the binding energies of the active center Cu^+ decrease in the order of $Cu_{II}Y > Cu_{II}Cs_{IIa^*}Y > Cu_{II}Cu_{IIa}Y > Cu_{II}Cu_{I'a}Y$, and

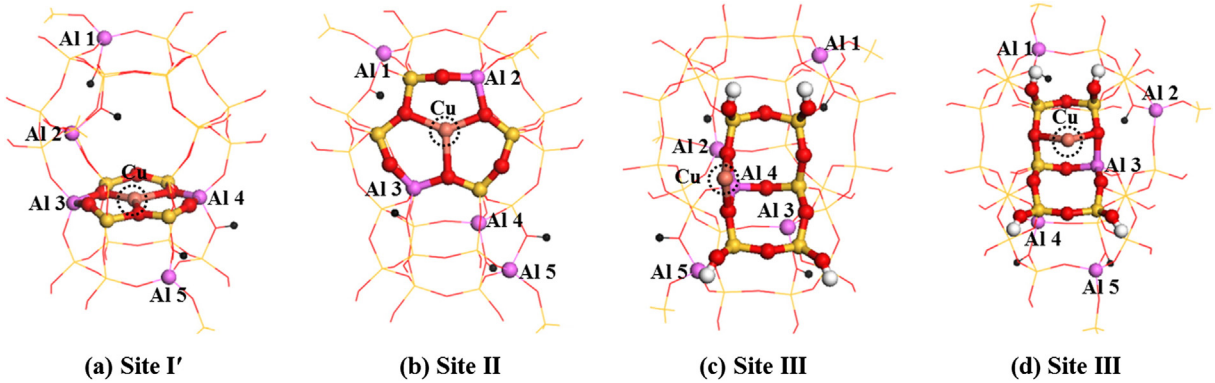

Fig. 5. The stable structures of Cu^+ species located at several cationic sites of Y zeolite. (a) Cu^+ located at site I′ near Al3 atom; (b) Cu^+ located at site II near Al2 atom; (c) Cu^+ located at site III near Al4 atom; (d) Cu^+ located at site III near Al3 atom. Orange balls (in the rings) stand for Cu atoms, and others see Fig. 4 for other color coding. (For interpretation of the references to color in this figure legend, the reader is referred to the web version of this article.)

Table 1
The binding energies (E_{bind}) and the net charge (q (Cu)) (e) of Cu^+ species, and the average bond lengths of Cu – O and Cu – Al bonds of Cu^+ species at different cationic sites of Y zeolite.

Location of Cu^+	Al location near Cu^+	E_{bind} (kJ·mol^{-1})	q (Cu) (e)	Bond length (Å)		
				Average Cu – O	Average Cu – Al	
I′	Al3[a]	691.20	0.351	2.118	3.112	3.04[e]
	Al4[a]	687.20	0.345	2.114	3.174	
II	Al2[a]	684.45	0.358	2.160	2.977	2.95[e]
	Al3[a]	677.73	0.327	2.187	2.949	
	Al4[b]	646.56	0.328	2.186	2.945	
III	Al3[c]	597.76	0.365	2.132	2.735	2.69[e]
	Al4[d]	625.21	0.476	2.039	2.689	

[a] Cu^+ species located adjacent to the 6MR with two Al atoms.
[b] Cu^+ species located adjacent to the 6MR with only one Al atom.
[c] Cu^+ species located above 4MR.
[d] Cu^+ species located in the edge of two 4MRs.
[e] The results of reference [25].

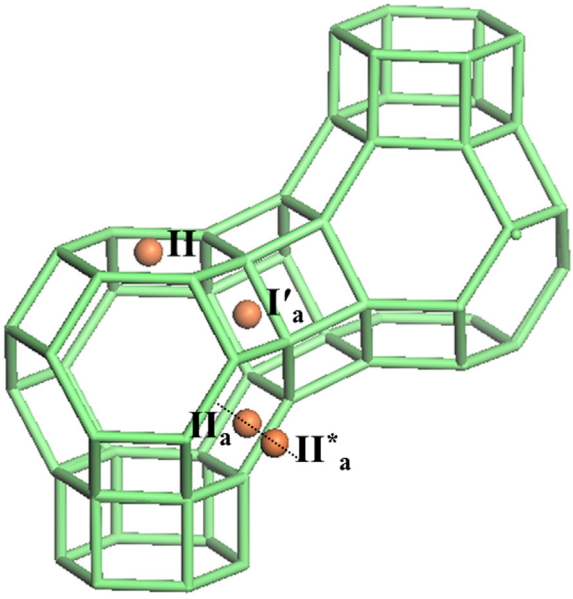

Fig. 6. The locations of sites I′, II, and II* (orange balls) adjacent to the active center Cu^+ at site II, denoted as I′$_a$, II$_a$, and II$_a$*, respectively. (For interpretation of the references to color in this figure legend, the reader is referred to the web version of this article.)

the HOMO–LUMO gap follows a similar trend, which agrees that the higher binding energy of Cu^+ is related to a larger HOMO–LUMO gap [45]. Consequently, the comparison results of various catalysts manifest that the differences of catalyst stability are related to the HOMO–LUMO gap, and the electronic properties of the active center Cu are influenced by its surrounding environment.

3.2. The adsorption of CO, CH_3OH and CH_3O on CuY zeolites with different environments

Previous studies [11,13,16] have pointed out that the adsorption of CO, CH_3OH, and CH_3O on CuY zeolite is related to the catalytic performance for DMC synthesis. The adsorption of CO on CuY zeolite is considered first. The stretching frequency (2113 cm^{-1}) and length (1.143 Å) of the C – O bond of CO in gas phase are calculated from our approach in accordance with the experimental values of 2125 cm^{-1} [47] and 1.128 Å [48], respectively, which also shows that the approach used in this study is reliable.

As shown in Fig. 8, CO molecule is linearly adsorbed by the C atom at the active center Cu^+ species of CuY zeolites with different environments. It can be also found that the adsorption of CO will lead to the shift of Cu^+ species from the plane of 6MR toward the supercage, and Cu^+ becomes twofold coordinated to O2 and O3 atoms of Y zeolite. Similar conclusions have been obtained by other researches [6,35,49,50]. Then, compared to 2113 cm^{-1} of CO in gas phase, the adsorption of CO leads to the significant blue shift of CO vibrational frequency to 2135 cm^{-1} of $Cu_{II}Y$, 2154 cm^{-1} of $Cu_{II}Cu_{IIa}Y$ and 2168 cm^{-1} of $Cu_{II}Cu_{I'a}Y$, which are in good accordance with 2139 cm^{-1} observed via IR spectroscopy [13,25]; meanwhile, their corresponding net charges of adsorbed CO are 0.425 e, 0.408 e and 0.426 e, respectively, suggesting that the electrons transfer from adsorbed CO to Cu^+. Deka et al. [51] have also proved that the blue shift of CO vibrational frequency may attribute to the electron transfer from 5σ orbital of CO to the empty orbital of Cu^+ cation. In addition, the C – O bond length is elongated from 1.143 Å in gas phase CO to 1.149 Å of $Cu_{II}Y$, 1.150 Å of $Cu_{II}Cu_{IIa}Y$ and 1.148 Å of $Cu_{II}Cu_{I'a}Y$ (see Fig. 8), indicating that the adsorption of CO weakens the C – O bond, and will contribute to the activation of CO.

The single adsorption of CH_3OH and CH_3O on CuY zeolites with different environments is also considered (see Fig. 8), and the corresponding calculated results are listed in Table 3. When oxygen is present in the feed, adsorbed CH_3OH can be converted rapidly to form CH_3O species over CuY zeolite [6,17]. As seen in Fig. 8, adsorbed CH_3OH and CH_3O on four types of catalysts are bound to the active center Cu^+ through O atom. It can be concluded from Table 3 that the adsorption energies of surface species on four catalysts increase in the order of CH_3OH < CO < CH_3O, suggesting that CO binds to the active center Cu^+ species more strongly than CH_3OH, while once CH_3O is formed, CH_3O species is the preferential adsorbed species and adsorbed CO is present as a minority species.

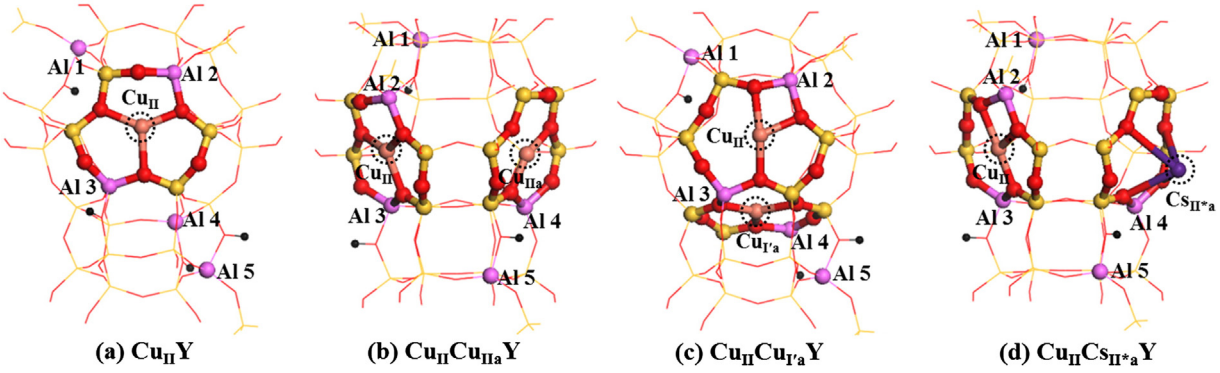

Fig. 7. The stable structures of $Cu_{II}Y$, $Cu_{II}Cu_{IIa}Y$, $Cu_{II}Cu_{I'a}Y$ and $Cu_{II}Cs_{IIa}$-Y zeolites. Purple and orange (in the rings) balls stand for Cs and Cu atoms, and others see Fig. 4 for the color coding. (For interpretation of the references to color in this figure legend, the reader is referred to the web version of this article.)

Table 2
The binding energies (E_{bind}), the net charge (q (Cu)) and the electronic configurations of the active center Cu^+ located at site II near Al2 atom, and HOMO–LUMO gaps of CuY zeolites with different environments.

Catalyst	E_{bind} (kJ·mol^{-1})	q (Cu)[a] (e)	Electronic configuration of Cu[b]	Gap (eV)
$Cu_{II}Y$	684.45	0.358	$3d^{9.951}4s^{0.441}4p^{0.25}$	0.09627
$Cu_{II}Cu_{IIa}Y$	671.99	0.365	$3d^{9.958}4s^{0.428}4p^{0.249}$	0.08874
$Cu_{II}Cu_{I'a}Y$	647.39	0.393	$3d^{9.953}4s^{0.425}4p^{0.229}$	0.07310
$Cu_{II}Cs_{IIa^*}Y$	673.21	0.345	$3d^{9.943}4s^{0.477}4p^{0.235}$	0.09029

[a] The net charge of the active center Cu^+ species at II.
[b] The electronic configuration of the active center Cu^+ species at II.

3.3. The co-adsorption of CO/CH_3O on CuY zeolites with different environments

Based on the stable configurations of adsorbed CO and CH_3O, the configurations of co-adsorbed CO/CH_3O on four types of CuY zeolites can be also obtained (see Fig. 9). The corresponding calculated results are given in Table 3. Taking $Cu_{II}Y$ zeolite for example, the co-adsorbed CO/CH_3O reduces the adsorption energy of CO from 137.93 kJ·mol^{-1} of adsorbed CO to 74.18 kJ·mol^{-1}, which indicates that the presence of CH_3O the on active center Cu^+ leads to the weaker adsorption of CO. Relative to the single adsorption of CO, the stretching vibrational frequency of co-adsorbed CO red shifts to 2130 cm^{-1}, and the corresponding net charge decreases from 0.425 e to 0.363 e. The former case is attributed to an increase in electron transfer from Cu^+ species to the π^* anti-bonding orbital of CO [6,13], which agrees to the decrease of net charge of CO in the latter case. In addition, in co-adsorbed CO/CH_3O system, the adsorption energy (140.13 kJ·mol^{-1}) of CH_3O is lower than that (157.07 kJ·mol^{-1}) of its single adsorption, and the corresponding length of $Cu-OCH_3$ is elongated from 1.818 Å to 1.885 Å, which is in favor of CO insertion.

For CuY zeolites with other environments, similar results and stable configurations for co-adsorbed CO/CH_3O have been obtained and shown in Table 3 and Fig. 9, respectively. For co-adsorbed CO/CH_3O on $Cu_{II}Cu_{IIa}Y$ zeolite (see Fig. 9(b)), the length (1.906 Å) of $Cu-OCH_3$ bond is longer than that (1.885 Å) of CuY zeolite. Meanwhile, compared to $Cu_{II}Y$ zeolite, the adsorption energy of co-adsorbed CO on $Cu_{II}Cu_{IIa}Y$ zeolite increases to 76.83 kJ·mol^{-1}, and that of co-adsorbed CH_3O decreases to 136.18 kJ·mol^{-1}. Similarly, for $Cu_{II}Cs_{IIa^*}Y$ zeolite, the co-adsorbed CO/CH_3O reduces the adsorption energy of CO from 153.66 kJ·mol^{-1} of CO single adsorption to 95.89 kJ·mol^{-1}, which is the largest adsorption energy of co-adsorbed CO among four types of catalysts. And the $Cu-OCH_3$ bond of co-adsorbed CH_3O is 1.911 Å, which is longer than CuY zeolite with other environments (see Fig. 9). Nevertheless, for $Cu_{II}Cu_{I'a}Y$ zeolite, the $Cu-OCH_3$ bond (1.844 Å) in co-adsorbed CO/CH_3O system is much shorter than 1.885 Å of $Cu_{II}Y$

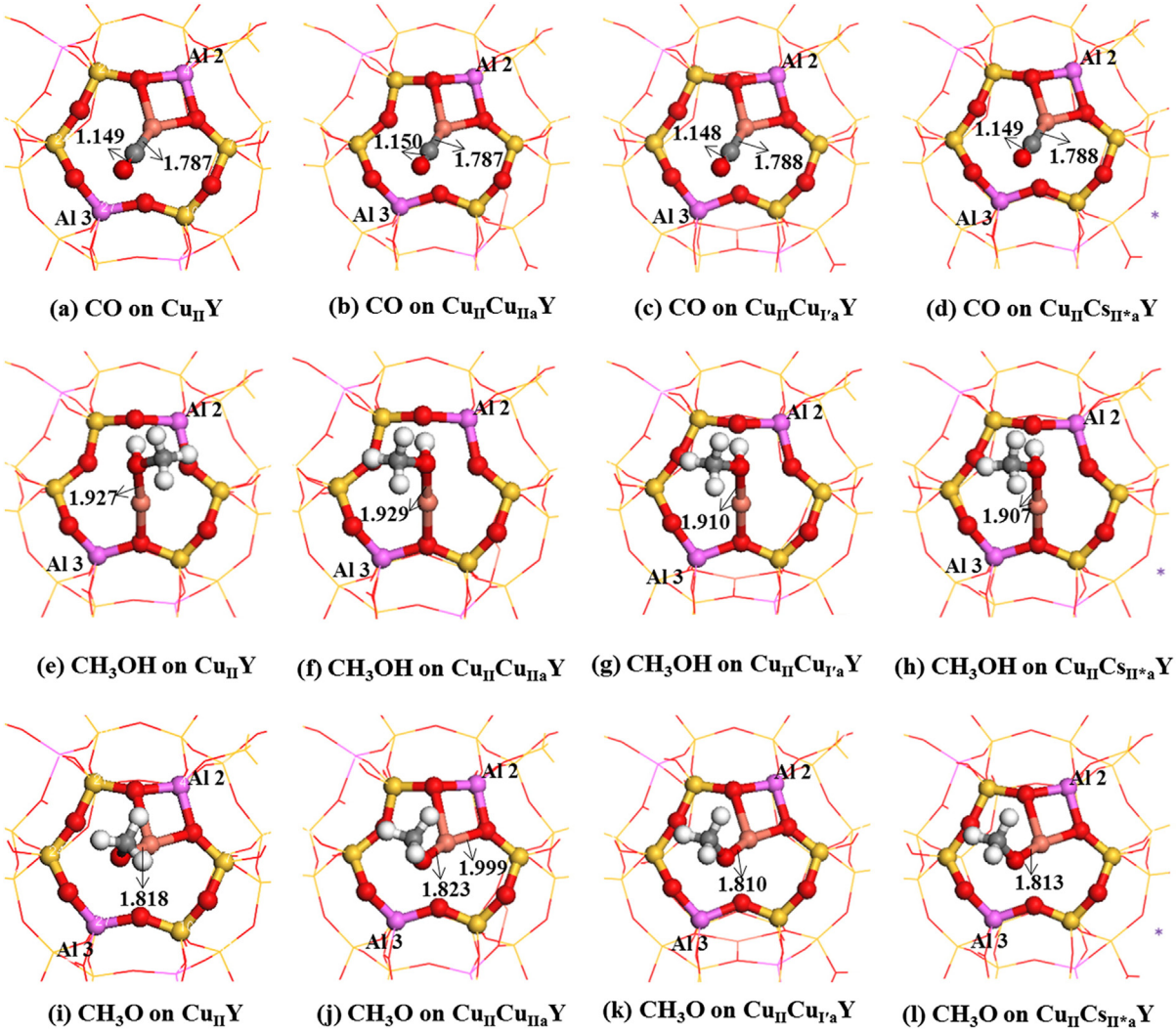

Fig. 8. The optimized stable adsorption configurations of single CO, CH_3OH and CH_3O species on $Cu_{II}Y$, $Cu_{II}Cu_{IIa}Y$, $Cu_{II}Cu_{I'a}Y$ and $Cu_{II}Cs_{IIa^*}Y$ catalysts, respectively (unit: Å). Orange and gray balls stand for Cu and C atoms, and others see Fig. 4 for the color coding. (For interpretation of the references to color in this figure legend, the reader is referred to the web version of this article.)

Table 3
The adsorption energies of single CH_3OH and adsorbed (co-adsorbed) CO (CH_3O) as well as the net charge (q (CO)) and the stretching vibrational frequencies (ν_{C-O}) of the adsorbed (co-adsorbed) CO on CuY zeolites with different environments.

Catalyst	Adsorbed CH_3OH	Adsorbed CO			Co-adsorbed CO			Adsorbed CH_3O	Co-adsorbed CH_3O
	E_{ads} (kJ·mol^{-1})	E_{ads} (kJ·mol^{-1})	ν_{C-O} (cm^{-1})	q (CO) (e)	E_{ads} (kJ·mol^{-1})	ν_{C-O} (cm^{-1})	q (CO) (e)	E_{ads} (kJ·mol^{-1})[1]	E_{ads} (kJ·mol^{-1})
$Cu_{II}Y$	86.91	137.93	2135	0.425	74.18	2130	0.363	157.07	140.13
$Cu_{II}Cu_{IIa}Y$	87.37	142.27	2154	0.408	76.83	2140	0.366	166.46	136.08
$Cu_{II}Cu_{I'a}Y$	103.17	154.40	2168	0.426	42.35	2140	0.395	177.32	110.10
$Cu_{II}Cs_{IIa^*}Y$	103.17	153.66	2094	0.409	95.89	2094	0.378	175.11	145.62

zeolite, which corresponds to the decrease of CO adsorption energy in co-adsorbed CO/CH_3O system from 74.18 kJ·mol^{-1} of $Cu_{II}Y$ zeolite to 42.35 kJ·mol^{-1}.

It can be concluded that the presence of Cu species at II_a or Cs species at II_a* improves the adsorption energy of co-adsorbed CO on the active center Cu^+, and elongates the Cu – OCH_3 bond of co-adsorption CO/CH_3O system, which can accommodate the insertion of CO much easier [25,52]. While Cu^+ species in the smallcage play opposite roles, the existence of Cu^+ species at I'_a restrains CO insertion.

3.4. The catalytic activity of CuY zeolites with different environments

As mentioned in the Introduction section, CO insertion into CH_3O to CH_3OCO is selected to evaluate the effect of environment around the active center Cu^+ species on the catalytic activity in DMC synthesis. The reaction of CO insertion into CH_3O to CH_3OCO goes through the formation of C – O bond with the C atom of CO binding to the O atom of CH_3O via a transition state (*TSn*). Based on the configurations of co-adsorbed CO/CH_3O and the adsorbed CH_3OCO, the reactions of CO insertion into CH_3O species over CuY zeolites with different environments are calculated by the LST/QST method.

It can be seen from the black line in Fig. 10 that CO insertion reaction over $Cu_{II}Y$ zeolite needs to overcome an activation barrier of 78.32 kJ·mol^{-1} via *TS1* (see Fig. 9(i)). For *TS1*, the distance of C atom to CO and O atoms of CH_3O decreases to 1.870 Å from 2.253 Å in the initial co-adsorbed CO/CH_3O, indicating that the C – O bond tends to be formed. In *TS1*, the adsorbed CO is activated with a C – O bond elongated to 1.180 Å, and the Cu – OCH_3 distance (2.250 Å) is much longer than that (1.885 Å) in the initial co-adsorbed CO/CH_3O, which is in favor of CO insertion. For $Cu_{II}Cu_{IIa}Y$ zeolite, CO insertion into CH_3O species needs to overcome a lower activation barrier of 64.59 kJ·mol^{-1} via *TS2* (see Fig. 9(j)), and this reaction is exothermic by 75.91 kJ·mol^{-1}. Similarly, for *TS2*, Cu – OCH_3 bond is elongated to 2.260 Å from 1.906 Å in the initial co-adsorbed CO/CH_3O, and the C – O length of CO increases to 1.179 Å. Nevertheless, for $Cu_{II}Cu_{I'a}Y$ zeolite, CO insertion reaction has an activation barrier of 138.96 kJ·mol^{-1} via *TS3* (see Fig. 9(k)) with the Cu – OCH_3 of 2.356 Å. For *TS3*, the corresponding C – O bond length (1.150 Å) of CO is slightly longer than that (1.145 Å) of CO in the initial co-adsorbed CO/CH_3O, suggesting that Cu^+ species at I'_a restrains the activation of CO, which is in agreement with a higher

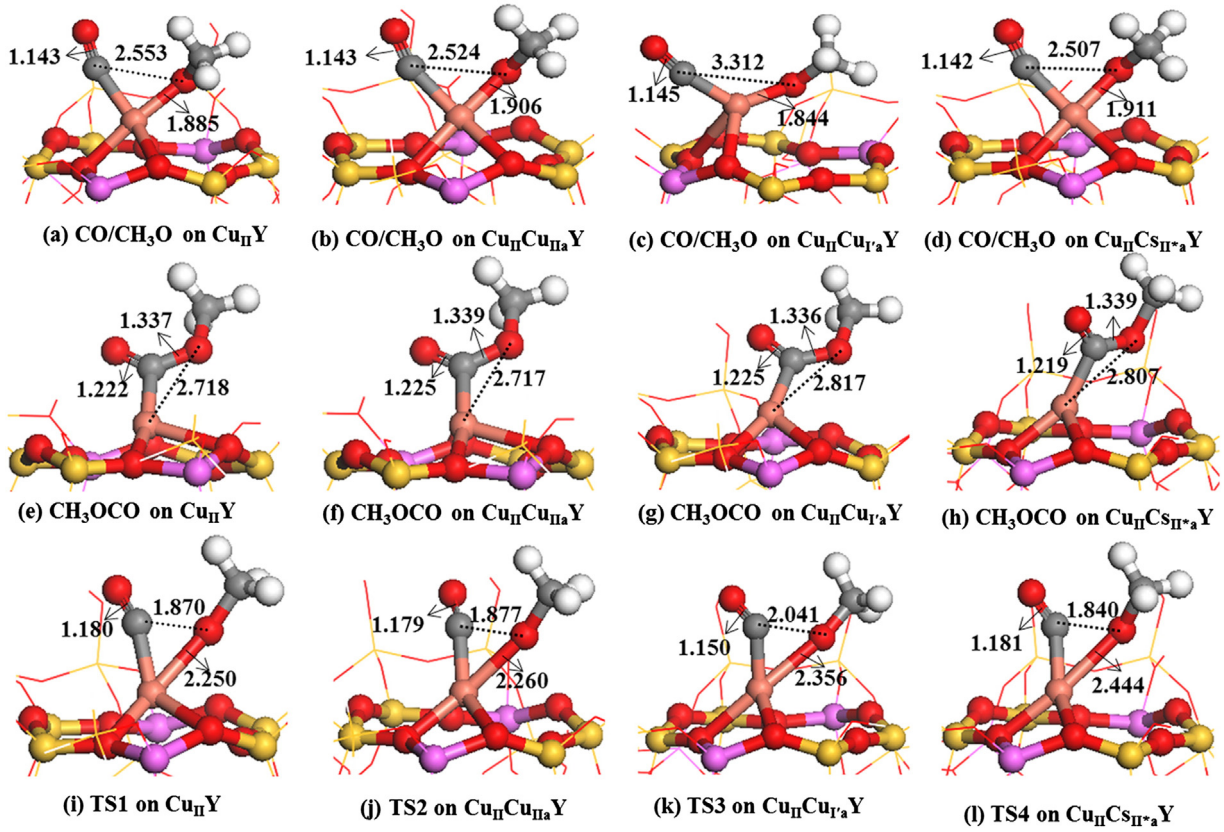

Fig. 9. Related structures of initial states, *TSn* (n = 1–4) and final states involved in CO insertion into CH_3O species to CH_3OCO on $Cu_{II}Y$, $Cu_{II}Cu_{IIa}Y$, $Cu_{II}Cu_{I'a}Y$ and $Cu_{II}Cs_{IIa^*}Y$ catalysts (unit: Å). See Fig. 8 for the color coding. (For interpretation of the references to color in this figure legend, the reader is referred to the web version of this article.)

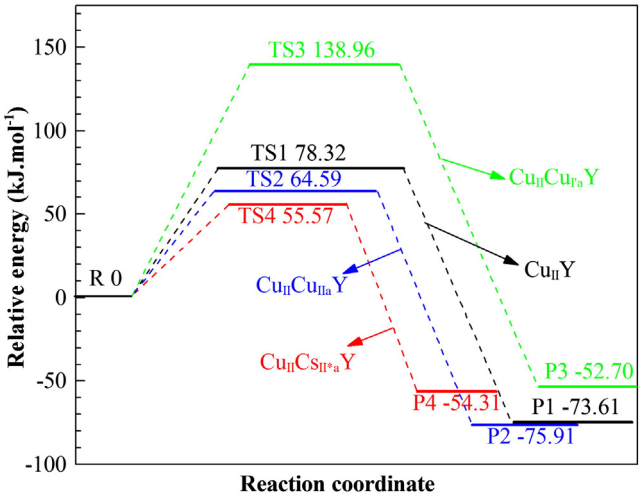

Fig. 10. Potential energy profiles for the reaction of CO insertion into CH_3O species to CH_3OCO over $Cu_{II}Y$, $Cu_{II}Cu_{IIa}Y$, $Cu_{II}Cu_{I'a}Y$ and $Cu_{II}Cs_{IIa*}Y$ catalysts. *TSn* ($n = 1$–4) represent the transition states involved in CO insertion into CH_3O species to CH_3OCO.

activation barrier of $Cu_{II}Cu_{I'a}Y$. For $Cu_{II}Cs_{IIa*}Y$ zeolite, CO insertion reaction needs to overcome an activation barrier of 55.57 kJ·mol^{-1} via *TS4* (see Fig. 9(l)) with the longest Cu – OCH_3 bond of 2.444 Å, indicating that CO can easily insert into CH_3O, which is corresponding with the highest catalytic activity of $Cu_{II}Cs_{IIa*}Y$ zeolite. In conclusion, the activation barriers of four types of catalysts decrease in the following order of $Cu_{II}Cu_{I'a}Y$, $Cu_{II}Y$, $Cu_{II}Cu_{IIa}Y$, and $Cu_{II}Cs_{IIa*}Y$ zeolites, indicating that the catalytic activity should be sensitive to the environment around the active center Cu^+ species.

In order to further probe into the effect of the environment, the adsorption energies of co-adsorbed CO/CH_3O, as well as transition states for the elementary reaction of CH_3OCO formation on four types of catalysts with different environments have been also calculated (see Table 4). It can be seen from Table 4 that the adsorption energies of co-adsorbed CO/CH_3O and *TS1* for the elementary reaction of CH_3OCO formation on $Cu_{II}Y$ zeolite are 211.03 and 132.52 kJ·mol^{-1}, respectively. For $Cu_{II}Cu_{IIa}Y$ zeolite, the adsorption energy (210.90 kJ·mol^{-1}) of co-adsorbed CO/CH_3O is similar to that on $Cu_{II}Y$ zeolite, but the adsorption energy of *TS2* on $Cu_{II}Cu_{IIa}Y$ zeolite increases to 146.55 kJ·mol^{-1}. For $Cu_{II}Cu_{I'a}Y$ zeolite, the adsorption energy (241.11 kJ·mol^{-1}) of CO/CH_3O is higher by 30.08 kJ·mol^{-1} than $Cu_{II}Y$ zeolite, and the adsorption energy (101.80 kJ·mol^{-1}) of *TS3* is lower by 30.72 kJ·mol^{-1} than $Cu_{II}Y$ zeolite. While the adsorption energy (167.19 kJ·mol^{-1}) of *TS4* on $Cu_{II}Cs_{IIa*}Y$ zeolite is the largest among four types of catalysts.

The calculated results confirm that the presence of Cu^+ species at the adjacent site II_a can well stabilize the configuration of *TS2*, achieving the enhanced ability of CO insertion; the existence of Cu^+ species at I'_a in the smallcage improves the stability of co-adsorbed CO/CH_3O configuration and destabilizes the *TS3* for the elementary reaction of CH_3OCO formation. In general, the high stability of transition state for the elementary reaction is related to the good catalytic activity of the reaction [52,53]. Therefore, the above analysis results account for the low activation barrier (64.59 kJ·mol^{-1}) for $Cu_{II}Cu_{IIa}Y$ zeolite, and the high one (138.96 kJ·mol^{-1}) for $Cu_{II}Cu_{I'a}Y$ zeolite, manifesting that $Cu_{II}Cu_{IIa}Y$ zeolite exhibits better catalytic activity. Furthermore, introducing Cs species furthest enhances the stability of *TS4* for the formation of CH_3OCO, as a result, the activation barrier of CO insertion reaction over $Cu_{II}Cs_{IIa*}Y$ zeolite decreases, and ultimately the catalytic activity of CuY zeolite for DMC synthesis is improved, which is in good agreement with our previous experimental results [29].

Table 4
The adsorption energies of co-adsorbed CO/CH_3O and *TS* involved in CO insertion into CH_3O to CH_3OCO over CuY zeolites with different environments.

Catalyst	E_{ads} (kJ·mol^{-1})	
	Co-adsorbed CO/CH_3O	*TSn*
$Cu_{II}Y$	211.03	132.52 (*TS1*)
$Cu_{II}Cu_{IIa}Y$	210.90	146.55 (*TS2*)
$Cu_{II}Cu_{I'a}Y$	241.11	101.80 (*TS3*)
$Cu_{II}Cs_{IIa*}Y$	222.59	167.19 (*TS4*)

4. Conclusions

In this study, DFT method has been employed to investigate the catalytic activity of the active center Cu^+ species with four types of environments in the oxidative carbonylation of methanol to DMC. The stable configurations of CuY zeolites reflecting different environments around Cu^+ species have been constructed. The results show that the order of catalytic activity is $Cu_{II}Cs_{IIa*}Y > Cu_{II}Cu_{IIa}Y > Cu_{II}Y > Cu_{II}Cu_{I'a}Y$. For the rate-limiting step of DMC formation, CO insertion into CH_3O to CH_3OCO, the presence of Cu^+ at II_a enhances the stability of the transition state, which exhibits better catalytic activity for DMC formation. Whereas, Cu^+ at I'_a in the smallcage destabilizes the transition state, and makes the active center Cu^+ exhibit lower catalytic activity; further, the migration of Cu species from the surpercage to smallcage decreases the amount of the active Cu species, and reduces the catalytic activity of CuY zeolites, namely, hindering the migration of Cu^+ species in the smallcage can improve the catalytic activity of CuY zeolites, this is an interesting finding to develop newly efficient CuY zeolites in DMC synthesis. Finally, compared to the above three types of CuY zeolites, the introduction of Cs species into the supercage greatly stabilizes the transition state, and exhibits the best catalytic activity among four types of CuY zeolites.

Acknowledgment

This work is supported by the National Natural Science Foundation of China (21106092, 21276169, 20936003).

References

[1] N. Keller, G. Rebmann, V. Keller, Catalysts, mechanisms and industrial processes for the dimethylcarbonate synthesis, Journal of Molecular Catalysis A: Chemical 317 (2010) 1–18.
[2] Y. Ono, Catalysis in the production and reactions of dimethyl carbonate, an environmentally benign building block, Applied Catalysis A: General 155 (1997) 133–166.
[3] Y. Ono, Dimethyl carbonate for environmentally benign reactions, Pure and Applied Chemistry 68 (1996) 367–375.
[4] F. Arico, P. Tundo, Dimethylcarbonate: a modern green reagent and solvent, Russian Chemical Reviews 79 (2010) 479–489.
[5] M.A. Pacheco, C.L. Marshall, Review of dimethyl carbonate (DMC) manufacture and its characteristics as a fuel additive, Energy & Fuels 11 (1997) 2–29.
[6] X.B. Zheng, A.T. Bell, A theoretical investigation of dimethyl carbonate synthesis on Cu–Y zeolite, The Journal of Physical Chemistry C 112 (2008) 5043–5047.
[7] Y.H. Zhang, I.J. Drake, D.N. Briggs, A.T. Bell, Synthesis of dimethyl carbonate and dimethoxy methane over Cu-ZSM-5, Journal of Catalysis 244 (2006) 219–229.
[8] U. Romano, R. Tesel, M.M. Mauri, P. Rebora, Synthesis of dimethyl carbonate from methanol, carbon monoxide, and oxygen catalyzed by copper compounds, Industrial & Engineering Chemistry Product Research and Development 19 (1980) 396–403.
[9] R. Jiang, Y. Wang, X. Zhao, S. Wang, C. Jin, C. Zhang, Characterization of catalyst in the synthesis of dimethyl carbonate by gas-phase oxidative carbonylation of methanol, Journal of Molecular Catalysis A: Chemical 185 (2002) 159–166.
[10] S.T. King, Oxidative carbonylation of methanol to dimethyl carbonate by solid-state ion-exchanged CuY catalysts, Catalysis Today 33 (1997) 173–182.
[11] S.A. Anderson, T.W. Root, Investigation of the effect of carbon monoxide on the oxidative carbonylation of methanol to dimethyl carbonate over Cu^+X and Cu^+ZSM-5 zeolites, Journal of Molecular Catalysis A: Chemical 220 (2004) 247–255.
[12] S.A. Anderson, T.W. Root, Kinetic studies of carbonylation of methanol to dimethyl carbonate over Cu^+X zeolite catalyst, Journal of Catalysis 217 (2003) 396–405.
[13] Y.H. Zhang, D.N. Briggs, E. Desmit, A.T. Bell, Effects of zeolite structure and composition on the synthesis of dimethyl carbonate by oxidative carbonylation of methanol on Cu-exchanged Y, ZSM-5, and mordenite, Journal of Catalysis 251 (2007) 443–452.
[14] Y. Shen, Q. Meng, S. Huang, S. Wang, J. Gong, X. Ma, Reaction mechanism of dimethyl carbonate synthesis on Cu/β zeolites: DFT and AIM investigations, RSC Advances 2 (2012) 7109–7119.
[15] S.T. King, Reaction mechanism of oxidative carbonylation of methanol to dimethyl carbonate in Cu–Y zeolite, Journal of Catalysis 161 (1996) 530–538.

[16] R. Zhang, J. Li, B. Wang, The effect of Si/Al ratios on the catalytic activity of CuY zeolites for DMC synthesis by oxidative carbonylation of methanol: a theoretical study, RSC Advances 3 (2013) 12287–12298.
[17] Y.H. Zhang, A.T. Bell, The mechanism of dimethyl carbonate synthesis on Cu-exchanged zeolite Y, Journal of Catalysis 255 (2008) 153–161.
[18] M. Richter, M. Fait, R. Eckelt, M. Schneider, J. Radnik, D. Heidemann, R. Fricke, Gas-phase carbonylation of methanol to dimethyl carbonate on chloride-free Cu-precipitated zeolite Y at normal pressure, Journal of Catalysis 245 (2007) 11–24.
[19] Z. Li, T.J. Fu, R.Y. Wang, Y.Y. Niu, H.Y. Zheng, Structure and catalytic active center of high catalytic activity CuY catalysts in oxidative carbonylation of methanol, Chemical Journal of Chinese Universities 32 (2011) 1366–1372.
[20] M. Richter, M.J.G. Fait, R. Eckelt, E. Schreier, M. Schneider, M.M. Pohl, R. Fricke, Oxidative gas phase carbonylation of methanol to dimethyl carbonate over chloride-free Cu-impregnated zeolite Y catalysts at elevated pressure, Applied Catalysis B: Environmental 73 (2007) 269–281.
[21] D. Berthomieu, G. Delahay, Recent advances in $Cu^{I/II}Y$: experiments and modeling, Catalysis Reviews: Science and Engineering 48 (2006) 269–313.
[22] W.M.H. Sachtler, Z. Zhang, Zeolite-supported transition metal catalysts, Advances in Catalysis 39 (1993) 129–220.
[23] H.S. Sherry, The ion-exchange properties of zeolites. I. Univalent ion exchange in synthetic faujasite, The Journal of Physical Chemistry 70 (1966) 1158–1168.
[24] G. Zi, H. Ming Yuan, D. Yi Yun, Zeolite Catalysis and Separation Technology, China Petrochemical Press, Beijing, 1999.
[25] I.J. Drake, Y. Zhang, D. Briggs, B. Lim, T. Chau, A.T. Bell, The local environment of Cu^{+} in Cu–Y zeolite and its relationship to the synthesis of dimethyl carbonate, The Journal of Physical Chemistry B 110 (2006) 11654–11664.
[26] J. Engeldinger, M. Richter, U. Bentrup, Mechanistic investigations on dimethyl carbonate formation by oxidative carbonylation of methanol over a CuY zeolite: an Operando SSITKA/DRIFTS/MS study, Physical Chemistry Chemical Physics 14 (2012) 2183–2191.
[27] I.E. Maxwell, J.J.d. Boer, Crystal structures and dehydrated divalent-copper-exchanged faujasite, The Journal of Physical Chemistry 79 (1975) 1874–1879.
[28] J.V. Smith, Faujasite-type structures: aluminosilicate framework: positions of cations and molecules: nomenclature, 101 (1974) 171–200.
[29] T. Fu, H. Zheng, Y. Niu, R. Wang, Z. Li, Effects of cerium, lanthanum and cesium cations on catalytic active center of CuY catalyst in oxidative carbonylation of methanol, Acta Chimica Sinica 69 (2011) 1765–1772.
[30] S. Kieger, G. Delahay, B. Coq, Influence of Co-cations in the selective catalytic reduction of NO by NH_3 over copper exchanged faujasite zeolites, Applied Catalysis B: Environmental 25 (2000) 1–9.
[31] M.F. Ribeiro, J.M. Silva, S. Brimaud, A.P. Antunes, E.R. Silva, A. Fernandes, P. Magnoux, D.M. Murphy, Improvement of toluene catalytic combustion by addition of cesium in copper exchanged zeolites, Applied Catalysis B: Environmental 70 (2007) 384–392.
[32] B. Delley, From molecules to solids with the $DMol^3$ approach, The Journal of Physical Chemistry 113 (2000) 7756–7764.
[33] J.P. Perdew, K. Burke, M. Ernzerhof, Generalized gradient approximation made simple, Physical Review Letters 77 (1996) 3865–3868.
[34] B. Delley, An all-electron numerical method for solving the local density functional for polyatomic molecules, The Journal of Physical Chemistry 92 (1990) 508–517.
[35] P. Rejmak, M. Sierka, J. Sauer, Theoretical studies of Cu(I) sites in faujasite and their interaction with carbon monoxide, Physical Chemistry Chemical Physics 9 (2007) 5446–5456.
[36] L. Kang, W. Deng, K. Han, T. Zhang, Z. Liu, A DFT study of adsorption hydrogen on the Li-FAU zeolite, International Journal of Hydrogen Energy 33 (2008) 105–110.
[37] G. Yang, Y. Wang, D. Zhou, X. Liu, X. Han, X. Bao, Density functional theory calculations on various M/ZSM-5 zeolites: interaction with probe molecule H_2O and relative hydrothermal stability predicted by binding energies, Journal of Molecular Catalysis A: Chemical 237 (2005) 36–44.
[38] S. Santra, T. Archipov, A.B. Ene, H. Komnik, H. Stoll, E. Roduner, G. Rauhut, Adsorption of dioxygen to copper in CuHY zeolite, Physical Chemistry Chemical Physics 11 (2009) 8855–8866.
[39] P. Rejmak, E. Broclawik, Nitrogen monoxide interaction with Cu(I) sites in zeolites X and Y: quantum chemical calculations and IR studies, The Journal of Physical Chemistry C 112 (2008) 17998–18010.
[40] J.-R. Hill, Clive M. Freeman, B. Delley, Bridging hydroxyl groups in faujasite: periodic vs cluster density functional calculations, The Journal of Physical Chemistry. A 103 (1999) 3772–3777.
[41] M. Sierka, U. Eichler, J. Datka, J. Sauer, Heterogeneity of Brønsted acidic sites in faujasite type zeolites due to aluminum content and framework structure, The Journal of Physical Chemistry B 102 (1998) 6397–6404.
[42] T. Frising, P. Leflaive, Extraframework cation distributions in X and Y faujasite zeolites: a review, Microporous and Mesoporous Materials 114 (2008) 27–63.
[43] S. Kieger, G. Delahay, B. Coq, B. Neveu, Selective catalytic reduction of nitric oxide by ammonia over Cu-FAU catalysts in oxygen-rich atmosphere, Journal of Catalysis 183 (1999) 267–280.
[44] D. Berthomieu, J.-M. Duce, A. Goursot, A theoretical study of Cu(II) sites in a faujasite-type zeolite: structures and electron paramagnetic resonance hyperfine coupling constants, The Journal of Physical Chemistry B 106 (2002) 7483–7488.
[45] D. Berthomieu, S. Krishnamurty, B. Coq, G. Delahay, A. Goursot, Theoretical modeling of a copper site in a Cu(II)–Y zeolite, The Journal of Physical Chemistry B 105 (2001) 1149–1156.
[46] M. Dolg, U. Wedig, H. Stoll, H. Preuss, Energy-adjusted ab initio pseudopotentials for the first row transition elements, The Journal of Chemical Physics 86 (1987) 866.
[47] J. Bak, S. Clausen, Signal-to-noise ratio of FT-IR CO gas spectra, Applied Spectroscopy 53 (1999) 697–700.
[48] J.X. Shao, X.L. Cheng, X.D. Yang, F.P. Zhang, S.H. Ge, Calculations of bond dissociation energies and bond lengths of C – H, C – N, C – O, N – N, Journal of Atomic and Molecular Physics 23 (2006) 80–84.
[49] N. Jardillier, E.A. Villagomez, G. Delahay, B. Coq, D. Berthomieu, Probing Cu^{I}-exchanged zeolite with CO: DFT modeling and experiment, The Journal of Physical Chemistry B 110 (2006) 16413–16421.
[50] Z. Nour, H. Petitjean, D. Berthomieu, Cooperative cation migrations upon CO addition in Cu^{I}- and alkali-exchanged faujasite: a DFT study, The Journal of Physical Chemistry C 114 (2010) 17802–17811.
[51] A. Deka, R.C. Deka, A. Choudhury, Adsorption of CO on gas phase and zeolite supported gold monomers: a computational study, Chemical Physics Letters 490 (2010) 184–188.
[52] R. Zhang, L. Song, B. Wang, Z. Li, A density functional theory investigation on the mechanism and kinetics of dimethyl carbonate formation on Cu_2O catalyst, Journal of Computational Chemistry 33 (2012) 1101–1110.
[53] R. Zhang, G. Wang, B. Wang, Insights into the mechanism of ethanol formation from syngas on Cu and an expanded prediction of improved Cu-based catalyst, Journal of Catalysis 305 (2013) 238–255.